This article has been accepted for publication in a future issue of this journal, but has not been fully edited. Content may change prior to final publication.

Reduced-Complexity Non-coherent Soft-Decision-Aided DAPSK Dispensing with Channel Estimation

Chao Xu, *Student Member, IEEE*, Dandan Liang, *Student Member, IEEE*,
Soon Xin Ng, *Senior Member, IEEE*, and Lajos Hanzo *Fellow, IEEE*

***Abstract*—Differential Amplitude Phase Shift Keying (DAPSK), which is also known as star-shaped QAM has implementational advantages not only due to dispensing with channel estimation, but also as a benefit of its low signal detection complexity. It is widely recognized that separately detecting the amplitude and the phase of a received DAPSK symbol exhibits a lower complexity than jointly detecting the two terms. However, since the amplitude and the phase of a DAPSK symbol are affected by the correlated magnitude fading and phase-rotations, detecting the two terms completely independently results in a performance loss, which is especially significant for soft-decision-aided DAPSK detectors relying on multiple receive antennas. Therefore, in this contribution, we propose a new soft-decision-aided DAPSK detection method, which achieves the optimum DAPSK detection capability at a substantially reduced detection complexity. More specifically, we link each *a priori* soft input bit to a specific part of the channel's output, so that only a reduced subset of the DAPSK constellation points has to be evaluated by the soft DAPSK detector. Our simulation results demonstrate that the proposed soft DAPSK detector exhibits a lower detection complexity than that of independently detecting the amplitude and the phase, while the optimal performance of DAPSK detection is retained.**

***Index Terms*—Reduced-complexity, Log-MAP, Max-Log-MAP, Soft-decision-aided detection, DAPSK, Star QAM, Iterative demapping and decoding.**

I. Introduction

It is widely recognized that soft-decision techniques are superior to hard-decision techniques. More explicitly, the classic QAM detector was further developed for processing soft bits, to show that the full potential of sophisticated coded modulation schemes can be beneficially exploited [1]. However, accurate Channel State Information (CSI) is required by coherent QAM detection for avoiding false phase-locking of the carrier-recovery scheme [2]–[6]. As a remedy, Differential Amplitude Phase Shift Keying (DAPSK), which is also known as Star QAM, was proposed in [7] in order to dispense with high-complexity CSI estimation and hence to eliminate the pilot-overhead. It is demonstrated in [8] that the low-complexity non-coherent schemes are particularly important in the context of relay-aided cooperative systems, where it is unrealistic to expect that the relay can altruistically estimate the source-relay channel.

The state-of-the-art channel decoding algorithms may be beneficially applied to the soft-decision-aided demodulators [1], [9]. More explicitly, the classic BCJR algorithm of [10] invoked the MAP algorithm for channel decoding. Following the conception of the Soft Output Viterbi Algorithm (SOVA) [11] for reducing the complexity of the MAP algorithm, substantial research efforts have been dedicated to channel codes. An outstanding invention was the classic Log-MAP algorithm [12], which operates the MAP algorithm in the logarithmic domain. The so-called Max-Log-MAP algorithm was also proposed in [12], which searched for the two maximum *a posteriori* symbol probabilities having their specific bit fixed to 1 and 0, respectively. In this paper, we focus our attention on the low-complexity Max-Log-MAP conceived for soft-decision-aided DAPSK detection.

Apart from dispensing with channel estimation, DAPSK schemes also benefit from a low signal detection complexity. It is widely recognized that separately detecting the amplitude and the phase of a received DAPSK symbol exhibits a lower complexity than the complexity of jointly detecting the two terms. Following this idea, the hard-decision-aided DAPSK demodulator and the soft-decision-aided DAPSK demodulator were proposed in [7] and [13], respectively. However, in fact, the ring amplitude fading and the fading-induced phase-rotations of a DAPSK symbol are correlated, hence the attempt of detecting the two terms completely independently results in a performance loss, which is especially significant for DAPSK detectors relying on multiple receive antennas. As a remedy, a novel soft-decision-aided DAPSK demodulator which jointly detects the amplitude and the phase was proposed in [14], but its detection complexity was substantially increased. *Against this background, the novel contributions of this paper are as follows:*

1) *We demonstrate that a performance loss is imposed by independently detecting the received amplitude and the received phase of hard-decision-aided DAPSK, when multiple receive antennas are employed. As a remedy, we propose a new hard DAPSK detection method, which detects the amplitude with the aid of the detected phase. As a result of this 'partially-joint' amplitude-phase de-*

The authors are with the School of Electronics and Computer Science, University of Southampton, Southampton, SO17 1BJ, U.K. (e-mail: {cx1g08,dl4e08,sxn,lh}@ecs.soton.ac.uk).

The research leading to these results has received funding from the European Union's Contero Project. The financial support of the EPSRC UK in the framework of the IU-ATC and that of the European Research Council's Advance Fellow Grant is also gratefully acknowledged.

tection, the optimal performance is retained.

2) *Secondly, we propose a new method for substantially reducing the detection complexity of the soft-decision-aided DAPSK detector of [14], which may be invoked by a variety of iterative demapping and decoding schemes. More specifically, we link each a priori soft input bit to a specific part of the channel's output, so that only a reduced subset of the DAPSK constellation points has to be evaluated by the soft DAPSK detector. Our simulation results demonstrate that the proposed soft DAPSK detector exhibits an even lower detection complexity than that of the separate amplitude-phase DAPSK detector of [13]. This is achieved without imposing any performance loss compared to the optimal joint amplitude-phase DAPSK detector of [14].*

The remainder of this paper is organized as follows. The hard-decision-aided DAPSK detector and the soft-decision-aided DAPSK detector are introduced in Secs. II and III, respectively. We provide simulation results in Sec. IV, while our conclusions are offered in Sec. V.

The following notations are used throughout the paper. M-DAPSK (M_A,M_P) represents an M-DAPSK scheme that has M_A ring-amplitudes and M_P phases, where we have $M = M_A M_P$. The number of modulated Bits Per Symbol (BPS) is given by $\bar{m} = \bar{m}_A + \bar{m}_P$, where $\bar{m}_A$ and $\bar{m}_P$ are the bits which are mapped to the ring-amplitude and to the phase, respectively. Furthermore, we use $(\cdot)^*$ to denote the conjugate of a complex symbol/vector, while $\|\cdot\|^2$ refers to the Euclidean norm of a vector/matrix. The subscript of a symbol (e.g. the subscript k in s_k) indicates the time index, while the superscript of a symbol (e.g. the superscript u in s^u) represents the modulation index.

II. Hard-Decision-Aided DAPSK Detection

A. DAPSK Modulation

The constellation diagram of the classic 16-DAPSK(2,8) scheme is portrayed in Fig. 1. We deliberately rotate all the DAPSK constellations of [3], [7], [13], [14] anti-clockwise by π/M_P, so that there are exactly $M/4$ constellation points in each quadrant. We will demonstrate in Sec. III that this feature is beneficial for our soft-decision-aided DAPSK detector design. Furthermore, Gray labelling is applied to all DAPSK schemes in this paper. The symmetry exhibited by the Gray-labelled DAPSK constellation diagram is the key to the detection complexity reduction.

Similar to the regular QAM schemes [3], the power of the modulated DAPSK symbols has to be normalized. If we denote the ring ratio as α, then the power normalization factor is given by $\left(\beta = \frac{\sum_{a=0}^{(M_A-1)} \alpha^{2a}}{M_A}\right)$. Note that in Rayleigh fading channels, the advantageous choice for ring ratios are $(\alpha = 2.0)$ for M-DAPSK (2,M_P) [14]–[16] and $(\alpha = 1.4)$ for M-DAPSK (4,M_P) [17], [18], respectively.

If we denote the transmitted DAPSK symbol as $x_k = \gamma_k \exp(j\psi_k)$, where γ_k and ψ_k refer to the amplitude and the phase, respectively, then the differential encoding may be

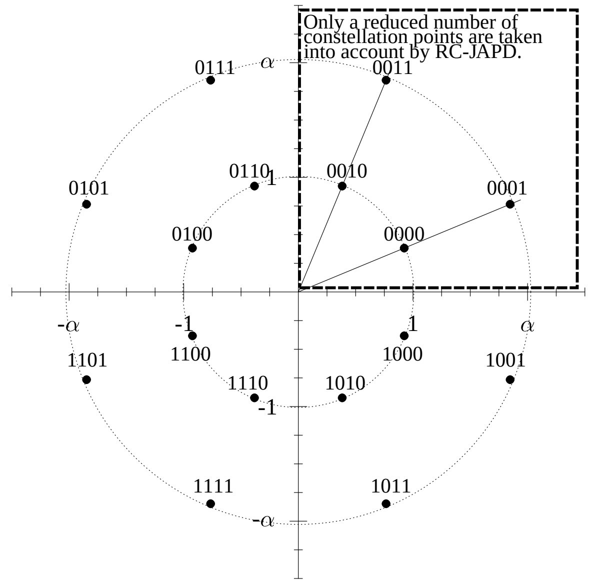

Fig. 1. Constellation diagram of 16-DAPSK (2,8). The constellation diagram of M-DAPSK (M_A, M_P) is rotated anti-clockwisely by π/M_P, so that there are exactly $M/4$ constellation points in each quadrant.

formulated as:

$$x_k = \begin{cases} \frac{1}{\sqrt{\beta}}, & \text{if } k = 0, \\ s_{k-1}x_{k-1}, & \text{if } k > 0, \end{cases} \tag{1}$$

where the modulated symbol $s_{k-1} = \frac{\gamma_k}{\gamma_{k-1}} \exp(j\Delta\psi_{k-1})$ carries the source information. More explicitly, a generic DAPSK modulator assigns the first $\bar{m}_P$ bits to modulate the phase difference of the transmitted symbols $\omega_{k-1} = \exp(j\Delta\psi_{k-1}) = \exp\left[j(\psi_k - \psi_{k-1})\right]$ as an M_P-PSK phasor, while the last $\bar{m}_A$ bits are assigned to modulate the amplitude difference of the transmitted symbols $\rho_{k-1} = \frac{\gamma_k}{\gamma_{k-1}}$ based on the previous ring amplitude γ_{k-1}. More specifically, for two-ring M-DAPSK (2,M_P) schemes, the amplitude difference is modulated as:

$$\rho_{k-1} = \begin{cases} \alpha^{-1}, & \text{if } b_{\bar{m}} = 1 \text{ and } \gamma_{k-1} = \frac{\alpha}{\sqrt{\beta}}, \\ 1, & \text{if } b_{\bar{m}} = 0, \\ \alpha, & \text{if } b_{\bar{m}} = 1 \text{ and } \gamma_{k-1} = \frac{1}{\sqrt{\beta}}, \end{cases} \tag{2}$$

while for four-ring M-DAPSK (4,M_P) schemes, the amplitude difference is modulated as:

$$\rho_{k-1} = \begin{cases} \alpha^{-3}, & \text{if } b_{\bar{m}-1}b_{\bar{m}} = 01 \text{ and } \gamma_{k-1} = \frac{\alpha^3}{\sqrt{\beta}}, \\ \alpha^{-2}, & \text{if } b_{\bar{m}-1}b_{\bar{m}} = 11 \text{ and } \gamma_{k-1} \in \{\frac{\alpha^2}{\sqrt{\beta}}, \frac{\alpha^3}{\sqrt{\beta}}\}, \\ \alpha^{-1}, & \text{if } b_{\bar{m}-1}b_{\bar{m}} = 10 \text{ and } \gamma_{k-1} \in \{\frac{\alpha}{\sqrt{\beta}}, \frac{\alpha^2}{\sqrt{\beta}}, \frac{\alpha^3}{\sqrt{\beta}}\}, \\ 1, & \text{if } b_{\bar{m}-1}b_{\bar{m}} = 00, \\ \alpha, & \text{if } b_{\bar{m}-1}b_{\bar{m}} = 01 \text{ and } \gamma_{k-1} \in \{\frac{1}{\sqrt{\beta}}, \frac{\alpha}{\sqrt{\beta}}, \frac{\alpha^2}{\sqrt{\beta}}\}, \\ \alpha^2, & \text{if } b_{\bar{m}-1}b_{\bar{m}} = 11 \text{ and } \gamma_{k-1} \in \{\frac{1}{\sqrt{\beta}}, \frac{\alpha}{\sqrt{\beta}}\}, \\ \alpha^3, & \text{if } b_{\bar{m}-1}b_{\bar{m}} = 10 \text{ and } \gamma_{k-1} = \frac{1}{\sqrt{\beta}}. \end{cases} \tag{3}$$

Since the amplitude difference ρ_{k-1} may be either equal to, smaller than or larger than one, depending on the previous ring amplitude γ_{k-1}, there are $(2M_A - 1)$ candidates for the amplitude difference ρ_{k-1} of a M-DAPSK(M_A,M_P) scheme, as seen in (2) and (3).

B. DAPSK Demodulation

Let us now consider an uplink scenario, where the transmitter is equipped with a single antenna, while the receiver relies on N_R receive antennas. For cooperative communication systems [8], [19], [20], N_R may refer to the number of relay nodes. Due to the increasing number of Virtual Antenna Array (VAA) links and the requirement of imposing a low signal processing complexity at the relay nodes, it becomes unrealistic to require accurate channel estimation, hence DAPSK is preferred. The received signal of the N_R receive antennas may be modelled as:

$$\mathbf{y}_k = x_k \mathbf{h}_k + \mathbf{n}_k, \tag{4}$$

where the N_R-element vectors $\mathbf{y}_k$, $\mathbf{h}_k$ and $\mathbf{n}_k$ model the received signal, the Rayleigh fading channels and the Additive White Gaussian Noise (AWGN), which has a zero mean and a variance of N_0 in each dimension, respectively. For Quasi-Static (QS) fading channels, we may assume $(\mathbf{h}_{k+1} = \mathbf{h}_k)$ over T_{QS} symbol periods. As a result, the next received signal vector may be expressed as:

$$\begin{aligned}\mathbf{y}_{k+1} &= x_{k+1}\mathbf{h}_k + \mathbf{n}_{k+1} \\ &= s_k \mathbf{y}_k + \widetilde{\mathbf{n}}_{k+1},\end{aligned} \tag{5}$$

where the equivalent noise term $(\widetilde{\mathbf{n}}_{k+1} = -s_k \mathbf{n}_k + \mathbf{n}_{k+1})$ is Gaussian-distributed with a zero mean and a variance of $(1+\rho_k^2)N_0$ in each dimension. Therefore, the corresponding hard-decision aided DAPSK detection may be expressed as:

$$\hat{s}_k = \arg\min_{s^u \in \mathbf{s}} \ \|\mathbf{y}_{k+1} - s^u \mathbf{y}_k\|^2, \tag{6}$$

where $\{s^u\}_{u=1}^{(2M_A-1)M_P}$ denotes the u-th element in the DAPSK symbols set $\mathbf{s}$. The demodulator of (6) operates on a vector-by-vector basis, where the detection complexity is increased, when the vector size is increased due to using more receive antennas. As a remedy, a decision variable may be introduced based on the Euclidean norm calculation of (6) as:

$$z_k = \mathbf{y}_{k+1} \cdot \mathbf{y}_k^* / \|\mathbf{y}_k\|^2. \tag{7}$$

Naturally, minimizing the metric $[\|\mathbf{y}_{k+1} - s^u\mathbf{y}_k\|^2 = \|\mathbf{y}_{k+1}\|^2 + |s^u|^2\|\mathbf{y}_k\|^2 - 2\text{Re}\{(s^u)^*\mathbf{y}_{k+1}\cdot\mathbf{y}_k^*\}]$ in (6) and minimizing $\left[|z_k - s^u|^2 = |z_k|^2 + |s^u|^2 - 2\text{Re}\{(s^u)^* z_k\}\right]$ are equivalent, because $\|\mathbf{y}_{k+1}\|^2$, $\|\mathbf{y}_k\|^2$ and $|z_k|^2$ are all invariant over the different candidates $s^u \in \mathbf{s}$. Therefore, the decision variable z_k may be used for detecting the amplitude and the phase of $s_k = \rho_k \omega_k$ separately as:

$$\hat{\rho}_k = \min_{\rho^v \in \rho} \ \left||z_k| - \rho^v\right|^2, \tag{8}$$

$$\hat{\omega}_k = \min_{\omega^l \in \omega} \ |z_k - \omega^l|^2, \tag{9}$$

where $\{\rho^v\}_{v=1}^{2M_A-1}$ and $\{\omega^l\}_{l=1}^{M_P}$ denote the v-th element in the ring amplitude subset ρ and the l-th element in the phasor subset ω, respectively. For the special case of $(N_R = 1)$, we have $|z_k| = \frac{|y_{k+1}\cdot y_k^*|}{|y_k|^2} = \frac{|y_{k+1}|}{|y_k|}$ and $\angle z_k = \angle \frac{z_k}{|z_k|} = \angle \frac{y_{k+1}\cdot y_k^*}{|y_{k+1}\cdot y_k^*|} = \angle y_{k+1} - \angle y_k$. Therefore, (8) and (9) are equivalent to the hard-decision-aided Star QAM detection introduced in [7].

However, the ML DAPSK detector of (6) and the simplified DAPSK detector of (8) and (9) do not have the same detection capability, as evidenced by Fig. 2, where the performance loss of (8) and (9) become significant, as N_R is increased. We will demonstrate in Sec. III that independently detecting the amplitude and the phase also results in a substantial performance degradation for soft-decision-aided DAPSK detection relying on multiple receive antennas.

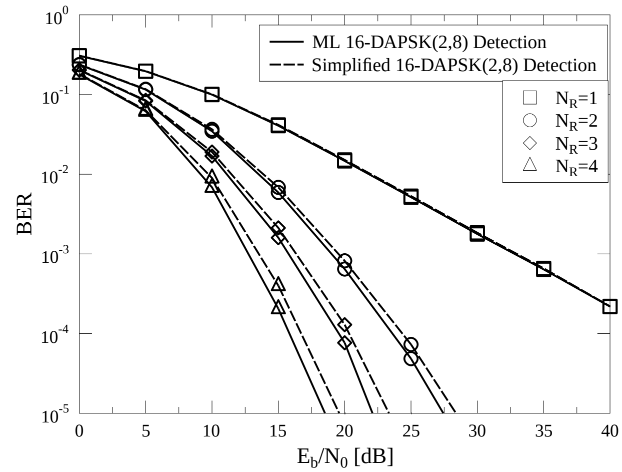

Fig. 2. Performance comparison between the ML DAPSK detecton of (6) and the simplified DAPSK detection of (8) and (9).

To elaborate a little further, the phase of a received DAPSK symbol may change the magnitudes on both the real and the imaginary axes of the received signal's constellation diagram, which implies that the detection of the amplitude in fact relies on the detection of the phase. Therefore, in order to restore the ML DAPSK detector's detection capability, we return to (6), which may be simplied as:

$$\begin{aligned}\{\hat{\rho}_k, \hat{\omega}_k\} &= \arg\min_{s^u \in \mathbf{s}} \ |s^u|^2 - 2\text{Re}\{(s^u)^* z_k\} \\ &= \arg\min_{\rho^v \in \rho, \omega^l \in \omega} \ (\rho^v)^2 - 2\rho^v \text{Re}\{(\omega^l)^* z_k\}.\end{aligned} \tag{10}$$

We define the local minimum metric of $[(\rho^v)^2 - 2\rho^v\text{Re}\{(\omega^l)^* z_k\}]$ in (10) as the minimum over the set of phasors $\omega^l \in \omega$ only, then (10) may be transformed to:

$$\begin{aligned}\hat{\omega}_k &= \arg\min_{\omega^l \in \omega} \ (\rho^v)^2 - 2\rho^v\text{Re}\{(\omega^l)^* z_k\} \\ &= \arg\min_{\omega^l \in \omega} \ -\text{Re}\{(\omega^l)^* z_k\},\end{aligned} \tag{11}$$

where a fixed amplitude is chosen from $\rho^v \in \rho$. After deleting the constants in (9), it can be seen that (11) and (9) have become equivalent. The global minimum in (10) may now be obtained by comparing the local minimum metrics, which may be expressed as:

$$\hat{\rho}_k = \arg\min_{\rho^v \in \rho} \ (\rho^v)^2 - 2\rho^v\text{Re}\{(\hat{\omega}_k)^* z_k\}, \tag{12}$$

where $\hat{\omega}_k$ is obtained by the local minimum search. As a result, (9) and (12) have exactly the same detection capability as (6). We have arranged for both detectors to process the same channel output, and they always produce the same decision. Moreover, (9) and (12) separately evaluate the phasor subset and the amplitude subset, so the low DAPSK detection complexity is retained.

III. Soft-Decision-Aided DAPSK Detection

A. Conventional Soft-Decision-Aided DAPSK Detection

In this section, we briefly summarize the features of the conventional soft-decision-aided DAPSK detectors, namely those of the Joint Amplitude-Phase Detector (JAPD) of [14] and those of the Separate Amplitude-Phase Detector (SAPD)[1] of [13].

The Log-MAP algorithm invoked by the JAPD produces the *a posteriori* LLR $L_p(b_m)$ as [12], [21]:

$$L_p(b_m) = \ln \frac{\sum_{s_k \in \mathbf{s}_{b_m=1}} \exp\left[d(\rho^v, \omega^l)\right]}{\sum_{s_k \in \mathbf{s}_{b_m=0}} \exp\left[d(\rho^v, \omega^l)\right]}, \tag{13}$$

where $\mathbf{s}_{b_m=1}$ and $\mathbf{s}_{b_m=0}$ represent the symbol set $\mathbf{s}$, when the specific bit b_m is fixed to 1 and 0, respectively, while the JAPD's probability metric $d(\rho^v, \omega^l)$ is defined as [14]:

$$d(\rho^v, \omega^l) = -\frac{\|\mathbf{y}_{k+1} - \rho^v w^l \mathbf{y}_k\|^2}{\widetilde{N}_0^v} + \sum_{\widetilde{m}=1}^{\bar{m}} b_{\widetilde{m}} L_a(b_{\widetilde{m}}), \tag{14}$$

where we have the equivalent noise power of $\{\widetilde{N}_0^v = \left[1 + (\rho^v)^2\right] N_0\}_{v=1}^{2M_A-1}$, while $\{L_a(b_{\widetilde{m}})\}_{\widetilde{m}=1}^{\bar{m}}$ denotes the *a priori* LLRs obtained from channel decoding. Similarly, the low-complexity Max-Log-MAP algorithm is formulated as [12]:

$$L_p(b_m) = \max_{s_k \in \mathbf{s}_{b_m=1}} \left[d(\rho^v, \omega^l)\right] - \max_{s_k \in \mathbf{s}_{b_m=0}} \left[d(\rho^v, \omega^l)\right], \tag{15}$$

where only the maximum *a posteriori* probability metrics are taken into account.

It can be seen that the Log-MAP of (13) and the Max-Log-MAP of (15) invoked by the JAPD have to evaluate $(2M_A - 1)M_P$ metrics $\{\{d(\rho^v, \omega^l)\}_{v=1}^{2M_A-1}\}_{l=1}^{M_P}$ of (14) in order to produce a single soft-bit decision. By contrast, the SAPD defines its amplitude-related probability metric $\{d(\rho^v)\}_{v=1}^{2M_A-1}$ and phase-related probability metric $\{d(\omega^l)\}_{l=1}^{M_P}$ separately as [13]:

$$\begin{aligned} d(\rho^v) = &\sum_{n=1}^{N_R} \left[\frac{-|y_{k+1}^n||y_k^n|}{N_0\left(1 + (\lambda_k^n)^2\right)} \left(\lambda_k^n - \rho^v\right)^2\right] \\ &+ \sum_{\widetilde{m}=\bar{m}_P+1}^{\bar{m}} b_{\widetilde{m}} L_a(b_{\widetilde{m}}), \end{aligned} \tag{16a}$$

$$\begin{aligned} d(\omega^l) = &\sum_{n=1}^{N_R} \left[-\frac{|y_{k+1}^n|^2 + |y_k^n|^2 (\lambda_k^n)^2}{N_0\left(1 + (\lambda_k^n)^2\right)} \right. \\ &\left. + \frac{2|y_{k+1}^n||y_k^n|\lambda_k^n \cos(\Delta\theta_k^n - \angle\omega^l)}{N_0\left(1 + (\lambda_k^n)^2\right)} \right] \\ &+ \sum_{\widetilde{m}=1}^{\bar{m}_P} b_{\widetilde{m}} L_a(b_{\widetilde{m}}), \end{aligned} \tag{16b}$$

where $\{y_k^n\}_{n=1}^{N_R}$ denotes the n-th element in $\mathbf{y}_k$, while we have $\lambda_k^n = |y_{k+1}^n|/|y_k^n|$ and $\Delta\theta_k^n = \angle y_{k+1}^n - \angle y_k^n$. The Log-MAP of (13) and the Max-Log-MAP of (15) invoked by the SAPD have only to evaluate and compare $(2M_A - 1)$ metrics $\{d(\rho^v)\}_{v=1}^{2M_A-1}$ of (16a) and M_P metrics $\{d(\omega^l)\}_{l=1}^{M_P}$ of (16b) for producing the amplitude bit decisions and the phase bit decisions. As a result, the SAPD exhibits a lower complexity.

If we use the Average Mutual Information (AMI) as a measure of detection capability, then the AMI achieved by the JAPD may be expressed as [13], [22]:

$$\begin{aligned} C_{JAPD} &= I(\mathbf{y}_{k+1}|\mathbf{y}_k; s_k) \\ &= \frac{1}{MM_A} \sum_{w=1}^{M_A} \sum_{u=1}^{M} \\ &\quad E\left\{\log_2\left[\frac{M \cdot p(\mathbf{y}_{k+1}|\mathbf{y}_k, \bar{s}^u)}{\sum_{\bar{u}=1}^{M} p(\mathbf{y}_{k+1}|\mathbf{y}_k, \bar{s}^{\bar{u}})}\right] \Big| s_k = \bar{s}^u, \gamma_k = \gamma^w\right\}, \end{aligned} \tag{17}$$

where $\{\gamma^w\}_{w=1}^{M_A}$ is taken from the M_A-element ring amplitudes set γ for γ_k, while $\{\bar{s}^u\}_{u=1}^{M}$ is taken from the M-element DAPSK symbol set $\bar{\mathbf{s}}$, whose size is smaller than the full set $\mathbf{s}$, simply because we have already decided upon the previous transmitted DAPSK symbol's amplitude $(\gamma_k = \gamma^w)$. Based on the received signal model of (5), the conditional probability seen in (17) is given by:

$$p(\mathbf{y}_{k+1}|\mathbf{y}_k, \bar{s}^u) = \frac{\exp\left[-\frac{\|\mathbf{y}_{k+1} - \bar{s}^u \mathbf{y}_k\|^2}{(1+|\bar{s}^u|^2)N_0}\right]}{\left[\pi(1 + |\bar{s}^u|^2)N_0\right]^{N_R}}. \tag{18}$$

Similarly, the AMI achieved by the SAPD [13], [22] is given by (19), where the conditions $(\gamma_k = \gamma^{w_1}, \gamma_{k+1} = \gamma^{w_2})$ and $(\gamma_k = \gamma^{w_1}, \gamma_{k+1} = \gamma^{\bar{w}_2})$ determine the amplitude variables ρ^v and $\rho^{\bar{v}}$, respectively, while the conditional probabilities in (19) are given by (20).

Based on (17) and (19), the AMI achieved by the JAPD and the SAPD is demonstrated in Fig. 3. It can be seen that the JAPD and the SAPD have a similar detection capability, when we have $(N_R = 1)$. However, the JAPD is capable of achieving a higher AMI, when multiple receive antennas are employed, as evidenced by Fig. 3 both for the 16-DAPSK(2,8) scheme and for the 64-DAPSK(4,16) arrangement.

B. Reduced-Complexity Soft-Decision-Aided DAPSK Detection

Since the *a posteriori* probability metrics $d(\rho^v, \omega^l)$ of (14) directly relate the symbol-level channel output $\left(-\frac{\|\mathbf{y}_{k+1} - \rho^v \omega^l \mathbf{y}_k\|^2}{\widetilde{N}_0^v}\right)$ to the symbol-level *a priori* LLRs $\left[\sum_{\widetilde{m}=1}^{\bar{m}} b_{\widetilde{m}} L_a(b_{\widetilde{m}})\right]$, the JAPD of Sec. III-A operates on a symbol-by-symbol basis, which implies that all the DAPSK constellation points have to be visited by the JAPD. Observe in Sec. II-B that instead of evaluating all the DAPSK constellation points using (6), the hard-decision-aided DAPSK detection of (9) and (12) tests only a reduced subset of the constellation points. Furthermore, the Max-Log-MAP of (15) aims for finding the maximum metric, which is similar to the action of the hard-decision-aided detection of (6). Motivated

[1] The SAPD refers to the final results of the Partially-combined Differential Detection (PDD) of [13]. Although the PDD's phase detector makes use of the received symbols' amplitudes, the PDD still evaluates the $(2M_A - 1)$-sized amplitude subset and the M_P-sized phase subset separately for detecting the $\bar{m}_A$ bits and the $\bar{m}_P$ bits, respectively. Therefore the PDD of [13] is referred to as SAPD in this paper.

$$
\begin{aligned}
C_{SAPD} &= I(\{\lambda_k^n\}_{n=1}^{N_R};\rho^v) + I(\{\Delta\theta_k^n,\lambda_k^n\}_{n=1}^{N_R};\omega^l) \\
&= \frac{1}{(M_A)^2}\sum_{w_1=1}^{M_A}\sum_{w_2=1}^{M_A} E\left\{\log_2\left[\frac{M_A\cdot p(\{\lambda_k^n\}_{n=1}^{N_R}|\rho^v)}{\sum_{\bar{w}_2=1}^{M_A} p(\{\lambda_k^n\}_{n=1}^{N_R}|\rho^{\bar{v}})}\right]\Big|\gamma_{k+1}=\gamma^{w_2},\gamma_k=\gamma^{w_1}\right\} \\
&\quad + \frac{1}{M}\sum_{w=1}^{M_A}\sum_{l=1}^{M_P} E\left\{\log_2\left[\frac{M_P\cdot p(\{\Delta\theta_k^n,\lambda_k^n\}_{n=1}^{N_R}|\omega^l)}{\sum_{\bar{l}=1}^{M_P} p(\{\Delta\theta_k^n,\lambda_k^n\}_{n=1}^{N_R}|\omega^{\bar{l}})}\right]\Big|\omega_k=\omega^l,\gamma_k=\gamma^w\right\},
\end{aligned}
\tag{19}
$$

$$
p(\{\lambda_k^n\}_{n=1}^{N_R}|\rho^v) = \prod_{n=1}^{N_R}\left\{\frac{N_0\lambda_k^n\left[1+(\lambda_k^n)^2\right]+\lambda_k^n|y_k^n|^2(\rho^v\lambda_k^n+1)^2}{\left[1+(\lambda_k^n)^2\right]^{\frac{5}{2}}\sqrt{\pi N_0|y_k^n|^2\lambda_k^n\rho^v}}\exp\left[\frac{-|y_k^n|^2}{N_0\left(1+(\lambda_k^n)^2\right)}\left(\lambda_k^n-\rho^v\right)^2\right]\right\},
\tag{20a}
$$

$$
\begin{aligned}
p(\{\Delta\theta_k^n,\lambda_k^n\}_{n=1}^{N_R}|\omega^l) = \prod_{n}^{N_R}\Big\{&\frac{\lambda_k^n}{\pi\left[1+(\lambda_k^n)^2\right]^2}\left[1+\frac{|y_{k+1}^n|^2(\lambda_k^n)^2+|y_k^n|^2+2\lambda_k^n|y_{k+1}^n||y_k^n|\cos(\Delta\theta_k^n-\angle\omega^l)}{N_0\left(1+(\lambda_k^n)^2\right)}\right] \\
&\times\exp\left[-\frac{|y_{k+1}^n|^2+|y_k^n|^2(\lambda_k^n)^2-2|y_{k+1}^n||y_k^n|\lambda_k^n\cos(\Delta\theta_k^n-\angle\omega^l)}{N_0\left(1+(\lambda_k^n)^2\right)}\right]\Big\}.
\end{aligned}
\tag{20b}
$$

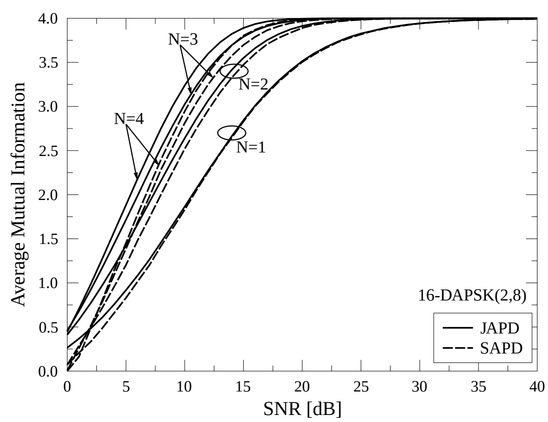

(a) 16-DAPSK(2,8)

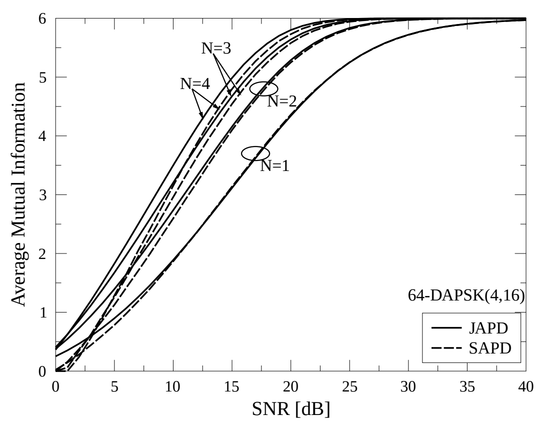

(b) 64-DAPSK(4,16)

Fig. 3. Comparison between AMI achieved by the JAPD of [14] and AMI achieved by the SAPD of [13]. The system parameters are summarized in Table IV.

by this, in this section, we aim for linking each *a priori* soft input bit to a specific part of the channel's output, so that only a reduced subset of the constellation points has to be evaluated by the JAPD. In the rest of this paper, we refer to the proposed Max-Log-MAP aided DAPSK detection as the Reduced-Complexity JAPD (RC-JAPD).

Considering 16-DAPSK (2,8) of Fig. 1 as our example, the Max-Log-MAP of (15) invoked for detecting the last bit b_4, which determines the ring amplitude, may be expressed as:

$$
\begin{aligned}
L_p(b_4) &= \max_{b_4=1}\ d(\rho^v,\omega^l) - \max_{b_4=0}\ d(\rho^v,\omega^l) \\
&= \max_{\omega^l\in\omega}\ \{d(\alpha^{-1},\omega^l), d(\alpha,\omega^l)\} - \max_{\omega^l\in\omega}\ d(1,\omega^l) \\
&= \max\ \{d_{\max}(\rho^1), d_{\max}(\rho^3)\} - d_{\max}(\rho^2),
\end{aligned}
\tag{21}
$$

where the local maximum probability metric of a specific ring amplitude index $v\in\{1,\cdots,2M_A-1\}$ is given by:

$$
d_{\max}(\rho^v) = \max_{\omega^l\in\omega}\ d(\rho^v,\omega^l). \tag{22}
$$

Similar to the hard-decision metric simplifications seen in (7), the *a posteriori* probability metric of (14) may be further extended as:

$$
\begin{aligned}
d(\rho^v,\omega^l) &= -\frac{\|\mathbf{y}_{k+1}\|^2}{\widetilde{N}_0^v} - \frac{(\rho^v)^2\|\mathbf{y}_k\|^2}{\widetilde{N}_0^v} \\
&\quad + \frac{2\rho^v\mathrm{Re}\{(\omega^l)^*\mathbf{y}_{k+1}\cdot\mathbf{y}_k^*\}}{\widetilde{N}_0^v} + \sum_{\widetilde{m}=1}^{\bar{m}} b_{\widetilde{m}}L_a(b_{\widetilde{m}}) \\
&= -\frac{\|\mathbf{y}_{k+1}\|^2}{\widetilde{N}_0^v} - \frac{(\rho^v)^2\|\mathbf{y}_k\|^2}{\widetilde{N}_0^v} + \frac{2\rho^v\mathrm{Re}(\omega^l)}{\widetilde{N}_0^v}\mathrm{Re}(\widetilde{z}_k) \\
&\quad + \frac{2\rho^v\mathrm{Im}(\omega^l)}{\widetilde{N}_0^v}\mathrm{Im}(\widetilde{z}_k) + \sum_{\widetilde{m}=1}^{\bar{m}} b_{\widetilde{m}}L_a(b_{\widetilde{m}}),
\end{aligned}
\tag{23}
$$

where we have the new decorrelating variable of ($\widetilde{z}_k = \mathbf{y}_{k+1}\cdot\mathbf{y}_k^*$). Therefore, the local maximum probability metric of (22) may be expressed as:

$$
d_{\max}(\rho^v) = \left[\max_{\omega^l\in\omega}\ \widetilde{d}(\rho^v,\omega^l)\right] + C_v, \tag{24}
$$

where we explicitly relate the amplitude index v to the corresponding *a priori* $L_a(b_4)$ by defining:

$$C_v = -\frac{\|\mathbf{y}_{k+1}\|^2}{\widetilde{N}_0^v} - \frac{(\rho^v)^2\|\mathbf{y}_k\|^2}{\widetilde{N}_0^v} + b_4 L_a(b_4), \quad (25)$$

while the remaining phasor-related sub-metric is given by:

$$\widetilde{d}(\rho^v, \omega^l) = \frac{2\rho^v \mathrm{Re}(\omega^l)}{\widetilde{N}_0^v}\mathrm{Re}(\widetilde{z}_k) + \frac{2\rho^v \mathrm{Im}(\omega^l)}{\widetilde{N}_0^v}\mathrm{Im}(\widetilde{z}_k) + \sum_{\bar{m}=1}^{\bar{m}_P} b_{\bar{m}} L_a(b_{\bar{m}}). \quad (26)$$

Let us now try to relate $L_a(b_2)$ and $L_a(b_1)$ to the real part and the imaginary part of the decorrelating variable $\widetilde{z}_k$, respectively. For a specific ring amplitude index v, there are $(M_P = 8)$ candidates for $\widetilde{d}(\rho^v, \omega^l)$. Considering the four candidates of $\omega^l \in \{\exp(\pm j\frac{\pi}{8}), \exp(\pm j\frac{7\pi}{8})\}$, which share the same coordinate magnitudes but are associated with different signs, the resultant four candidates of $\widetilde{d}(\rho^v, \omega^l)$ seen in (26) may be expressed as shown in (27), where we relate $\mathrm{Re}(\widetilde{z}_k)$ and $\mathrm{Im}(\widetilde{z}_k)$ to the corresponding *a priori* LLRs $L_a(b_2)$ and $L_a(b_1)$ by defining the following two test-variables as:

$$t^v_{\mathrm{Re}_1} = \frac{2\rho^v \cos(\frac{\pi}{8})}{\widetilde{N}_0^v}\mathrm{Re}(\widetilde{z}_k) - \frac{L_a(b_2)}{2},$$
$$t^v_{\mathrm{Im}_1} = \frac{2\rho^v \sin(\frac{\pi}{8})}{\widetilde{N}_0^v}\mathrm{Im}(\widetilde{z}_k) - \frac{L_a(b_1)}{2}. \quad (28)$$

It may be seen in (27) that all the four probability sub-metrics are constituted by three parts, i.e. they are $(\pm t^v_{\mathrm{Re}_1})$, $(\pm t^v_{\mathrm{Im}_1})$ as well as a constant of $\left[\frac{L_a(b_1)+L_a(b_2)}{2}\right]$. According to our arrangement, the only difference between the four candidates is the signs of the real and the imaginary test-variables. Therefore, the local maximum sub-metric over $\omega^l \in \{\exp(\pm j\frac{\pi}{8}), \exp(\pm j\frac{7\pi}{8})\}$ is directly given by:

$$\begin{aligned}\widetilde{d}_{\max_1}(\rho^v) &= \max_{\omega^l \in \{\exp(\pm j\frac{\pi}{8}), \exp(\pm j\frac{7\pi}{8})\}} \widetilde{d}(\rho^v, \omega^l) \\ &= \left|t^v_{\mathrm{Re}_1}\right| + \left|t^v_{\mathrm{Im}_1}\right| + \frac{L_a(b_1)+L_a(b_2)}{2}.\end{aligned} \quad (29)$$

Therefore, instead of evaluating and comparing a group of four probability sub-metrics in (27), the direct calculation of (29) may provide a significant 75% complexity reduction.

Similarly, the other local maximum sub-metric over $\omega^l \in \{\exp(\pm j\frac{3\pi}{8}), \exp(\pm j\frac{5\pi}{8})\}$ may also be given by a one-step calculation as:

$$\widetilde{d}_{\max_2}(\rho^v) = \left|t^v_{\mathrm{Re}_2}\right| + \left|t^v_{\mathrm{Im}_2}\right| + L_a(b_3) + \frac{L_a(b_1)+L_a(b_2)}{2}, \quad (30)$$

where the two new test-variables are defined by:

$$t^v_{\mathrm{Re}_2} = \frac{2\rho^v \sin(\frac{\pi}{8})}{\widetilde{N}_0^v}\mathrm{Re}(\widetilde{z}_k) - \frac{L_a(b_2)}{2},$$
$$t^v_{\mathrm{Im}_2} = \frac{2\rho^v \cos(\frac{\pi}{8})}{\widetilde{N}_0^v}\mathrm{Im}(\widetilde{z}_k) - \frac{L_a(b_1)}{2}. \quad (31)$$

After considering all the $(M_P = 8)$ phasors, the local maximum probability metric associated with a specific ring radius index v seen in (22) is now given by:

$$d_{\max}(\rho^v) = \left[\max_{i \in \{1,\cdots,M_P/4\}} \widetilde{d}_{\max_i}(\rho^v)\right] + C_v, \quad (32)$$

where $i \in \{1, \cdots, M_P/4\}$ denotes the phasor index for the M-DAPSK constellation points in the first quadrant, and then the global maximum metric persued by the Max-Log-MAP of (21) may be obtained by invoking (32). Moreover, we note that $\left(\frac{L_a(b_1)+L_a(b_2)}{2}\right)$ may be omitted in (29) and (30), because it is a common constant for all probability metrics $\{d_{\max}(\rho^v)\}_{v=1}^{2M_A-1}$ and hence it is eliminated by the negative polarity seen in the Max-Log-MAP of (21).

Since we have related $L_a(b_2)$ and $L_a(b_1)$ to the real and the imaginary parts of the decorelating variable, the local maximum sub-metric over every set of four probability sub-metrics which share the same magnitudes but are associated with different polarities is obtained in a single step in (29) and (30). This implies that only the $(M_P/4)$ specific phasors in the first quadrant have to be considered by the Max-Log-MAP, which is portrayed by Fig. 1.

More explicitly, we summarize the RC-JAPD proposed for the general M-DAPSK(M_A,M_P) scheme as in Algorithm 1.

Algorithm 1: RC-JAPD Detecting an M-DAPSK (M_A,M_P) Symbol.

1) Update the constants $\{C_v\}_{v=1}^{2M_A-1}$, which relate the last $\bar{m}_A$ *a priori* LLRs $\{L_a(b_{\bar{m}})\}_{\bar{m}=\bar{m}_P+1}^{\bar{m}}$ to the ring amplitude index v as:

$$C_v = -\frac{\|\mathbf{y}_{k+1}\|^2}{\widetilde{N}_0^v} - \frac{(\rho^v)^2\|\mathbf{y}_k\|^2}{\widetilde{N}_0^v} + \sum_{\bar{m}=\bar{m}_P+1}^{\bar{m}} b_{\bar{m}} L_a(b_{\bar{m}}), \quad (33)$$

where $\left(-\frac{\|\mathbf{y}_{k+1}\|^2}{\widetilde{N}_0^v}\right)$ only has to be estimated once and $\left(-\frac{\|\mathbf{y}_k\|^2}{\widetilde{N}_0^v}\right)$ is known from detecting the previous received signal block.

2) Evaluate the test-variables, which relate $L_a(b_2)$ and $L_a(b_1)$ to the real and imaginary parts of the decorrelating variable $(\widetilde{z}_k = \mathbf{y}_{k+1} \cdot \mathbf{y}_k^*)$ as:

$$t^v_{\mathrm{Re}_i} = \frac{2\rho^v a_i}{\widetilde{N}_0^v}\mathrm{Re}(\widetilde{z}_k) - \frac{L_a(b_2)}{2},$$
$$t^v_{\mathrm{Im}_i} = \frac{2\rho^v b_i}{\widetilde{N}_0^v}\mathrm{Im}(\widetilde{z}_k) - \frac{L_a(b_1)}{2}, \quad (34)$$

where $\{(a_i, b_i)\}_{i=1}^{M_P/4}$ are coordinates of the M_P-PSK phasors in the first quadrant.

3) Evaluate the local maximum sub-metric for each group, which relates the rest of the *a priori* LLRs $\{L_a(b_{\bar{m}})\}_{\bar{m}=3}^{\bar{m}_P}$ to the M_P-PSK phasor index $i \in \{1, \cdots, M_P/4\}$ as:

$$\widetilde{d}_{\max_i}(\rho^v) = \left|t^v_{\mathrm{Re}_i}\right| + \left|t^v_{\mathrm{Im}_i}\right| + \sum_{\bar{m}=3}^{\bar{m}_P} b_{\bar{m}} L_a(b_{\bar{m}}), \quad (35)$$

so that the local maximum metric associated with a specific ring index v may be obtained by:

$$d_{\max}(\rho^v) = \left[\max_{i \in \{1,\cdots,M_P/4\}} \widetilde{d}_{\max_i}(\rho^v)\right] + C_v. \quad (36)$$

$$\begin{aligned}
\widetilde{d}\left(\rho^v, \exp(j\tfrac{\pi}{8})\right) &= \tfrac{2\rho^v \cos(\frac{\pi}{8})}{\widetilde{N}_0^v}\mathrm{Re}(\widetilde{z}_k) + \tfrac{2\rho^v \sin(\frac{\pi}{8})}{\widetilde{N}_0^v}\mathrm{Im}(\widetilde{z}_k) &&= t^v_{\mathrm{Re}_1} + t^v_{\mathrm{Im}_1} + \tfrac{L_a(b_1)+L_a(b_2)}{2},\\
\widetilde{d}\left(\rho^v, \exp(j\tfrac{7\pi}{8})\right) &= -\tfrac{2\rho^v \cos(\frac{\pi}{8})}{\widetilde{N}_0^v}\mathrm{Re}(\widetilde{z}_k) + \tfrac{2\rho^v \sin(\frac{\pi}{8})}{\widetilde{N}_0^v}\mathrm{Im}(\widetilde{z}_k) + L_a(b_2) &&= -t^v_{\mathrm{Re}_1} + t^v_{\mathrm{Im}_1} + \tfrac{L_a(b_1)+L_a(b_2)}{2},\\
\widetilde{d}\left(\rho^v, \exp(-j\tfrac{\pi}{8})\right) &= \tfrac{2\rho^v \cos(\frac{\pi}{8})}{\widetilde{N}_0^v}\mathrm{Re}(\widetilde{z}_k) - \tfrac{2\rho^v \sin(\frac{\pi}{8})}{\widetilde{N}_0^v}\mathrm{Im}(\widetilde{z}_k) + L_a(b_1) &&= t^v_{\mathrm{Re}_1} - t^v_{\mathrm{Im}_1} + \tfrac{L_a(b_1)+L_a(b_2)}{2},\\
\widetilde{d}\left(\rho^v, \exp(-j\tfrac{7\pi}{8})\right) &= -\tfrac{2\rho^v \cos(\frac{\pi}{8})}{\widetilde{N}_0^v}\mathrm{Re}(\widetilde{z}_k) - \tfrac{2\rho^v \sin(\frac{\pi}{8})}{\widetilde{N}_0^v}\mathrm{Im}(\widetilde{z}_k) + L_a(b_1) + L_a(b_2) &&= -t^v_{\mathrm{Re}_1} - t^v_{\mathrm{Im}_1} + \tfrac{L_a(b_1)+L_a(b_2)}{2}.
\end{aligned} \tag{27}$$

4) The soft-bit output for the last $\bar{m}_A$ bits is directly given by:

$$L_p(b_m) = \max_{b_m=1} \; d_{\max}(\rho^v) - \max_{b_m=0} \; d_{\max}(\rho^v), \quad m \in \{\bar{m}_P+1, \cdots, \bar{m}\}, \tag{37}$$

where the tentative indices set for $[v \in \{1, \cdots, 2M_A - 1\}]$ is divided into two subsets corresponding to fixing the specific bit b_m to 1 and 0, respectively. Considering 16-DAPSK(2,8) as an example, the subsets for index v are given by $(v \in \{1, 3\})$ and $(v = 2)$, when we fix b_4 to 1 and 0, respectively, as seen in (21).

5) When detecting the first two bits which determine the quadrant, (37) is replaced by:

$$L_p(b_m) = \max_{b_m=1} \; d_{\max}(\rho^v) - \max_{b_m=0} \; d_{\max}(\rho^v), \quad m \in \{1, 2\}. \tag{38}$$

Furthermore, when a specific bit is fixed to $\{b_m = b\}_{m=1}^2$, where we have $b \in \{1, 0\}$, the constellation set for ω^l is halved, and hence Step 3 should be updated for (38) accordingly. For example, when $(b_1 = 1)$ is fixed, only the constellation points on the lower half of the constellation plane of Fig. 1 have to be considered, and hence $\left|t^v_{\mathrm{Im}_i}\right|$ has to be replaced by $-t^v_{\mathrm{Im}_i}$ in (35). When $(b_1 = 0)$ is fixed, $\left|t^v_{\mathrm{Im}_i}\right|$ has to be replaced by $t^v_{\mathrm{Im}_i}$. Similarly, when the second bit b_2 is fixed to 1 or 0, $\left|t^v_{\mathrm{Re}_i}\right|$ in (35) should be replaced by $-t^v_{\mathrm{Re}_i}$ or $t^v_{\mathrm{Re}_i}$, respectively.

6) When detecting the middle $(\bar{m}_P - 2)$ bits, which determine the $(M_P/4)$ M_P-PSK phasors in the first quadrant, (37) may be replaced by:

$$L_p(b_m) = \max_{b_m=1} \; d_{\max}(\rho^v) - \max_{b_m=0} \; d_{\max}(\rho^v), \quad m \in \{3, \cdots, \bar{m}_P\}. \tag{39}$$

For a specific subset of ω^l defined by fixing $\{b_m = b\}_{m=3}^{\bar{m}_P}$, the phasor index i seen in (36) is updated as:

$$d_{\max}(\rho^v) = \left[\max_{b_m=b} \; \widetilde{d}_{\max_i}(\rho^v)\right] + C_v, \tag{40}$$

where the phasor index set of $(i \in \{1, \cdots, M_P/4\})$ is halved, when a specific bit $(b_m = b)$ is fixed. Considering 16-DAPSK(2,8) as an example, we have $\left[d_{\max}(\rho^v) = \widetilde{d}_{\max_2}(\rho^v) + C_v\right]$ for (40) if $(b_3 = 1)$ is fixed, where only $(i = 2)$ is considered. By contrast, only $(i = 1)$ should be considered when $(b_3 = 0)$ is fixed, which results in the simple relationship of $\left[d_{\max}(\rho^v) = \widetilde{d}_{\max_1}(\rho^v) + C_v\right]$.

C. Complexity Analysis

In this section, we provide our complexity analysis for the three soft-decision-aided DAPSK detectors in terms of both the number of constellation points visited by the detectors as well as the total number of real-valued calculations contributed by the detectors.

According to Sec. III-A, the total number of constellation points visited by the conventional JAPD is given by $\left[N_{vc}^{JAPD} = (2M_A - 1)M_P\right]$. By contrast, the SAPD evaluates the amplitude subset and the phasor subset separately, so the total number of constellation points visited by the SAPD may be expressed by $\left[N_{vc}^{SAPD} = (2M_A - 1) + M_P\right]$. Furthermore, as portrayed by Fig. 1, the proposed RC-JAPD visits a reduced number of the DAPSK constellation points, which is given by $\left[N_{vc}^{RC-JAPD} = (2M_A - 1)M_P/4\right]$.

More specifically, for 16-DAPSK(2,8), the JAPD visits $(N_{vc}^{JAPD} = 24)$ constellation points, which is higher than $(N_{vc}^{SAPD} = 11)$ of the SAPD, but the lowest is given by $(N_{vc}^{RC-JAPD} = 6)$ of the proposed RC-JAPD. For 64-DAPSK(4,16), our proposed RC-JAPD visits $(N_{vc}^{RC-JAPD} = 28)$ constellation points, which is substantially lower than $(N_{vc}^{JAPD} = 112)$, but $N_{vc}^{RC-JAPD}$ is still slightly higher than $(N_{vc}^{SAPD} = 23)$.

Since the DAPSK detectors are implemented by obeying different equations, we quantify the complexity in terms of the total number of real-valued calculations required for producing a single-bit decision. We note that the JAPD and the SAPD aided DAPSK detection complexity increases multiplicatively as N_R increases, owing to the fact that all the *a posteriori* probabilities at the N_R antennas have to be multiplied together, as illustrated by (14) and (16). By contrast, the proposed RC-JAPD utilizes the decorrelating variable of $(\widetilde{z}_k = \mathbf{y}_{k+1} \cdot \mathbf{y}_k^*)$, which implies that all the detection procedures after Step 2 of Algorithm 1 have exactly the same detection complexity as a single-antenna-based detector.

We provide our complexity comparison between different DAPSK detectors in Fig. 4, which shows that the JAPD generally exhibits a higher complexity than the SAPD. However, a significant $74.7\% \sim 89.6\%$ complexity reduction is achieved by the proposed RC-JAPD compared to the JAPD using the Max-Log-MAP, both for 16-DAPSK(2,8) and for 64-DAPSK(4,16). As a result, for 16-DAPSK(2,8) detection, the RC-JAPD imposes the lowest detection complexity, as evidenced by Fig. 4(a), owing to the fact that RC-JAPD visits the lowest number of constellation points in this case. Furthermore, observe in Fig. 4(b) for 64-DAPSK(4,16) that the proposed RC-JAPD still exhibits a slightly higher complexity than the SAPD using the Max-Log-MAP, when we have $(N_R = 1)$, because $(N_{vc}^{RC-JAPD} = 28)$ is higher than $(N_{vc}^{SAPD} = 23)$ for 64-DAPSK(4,16). However, as N_R increases, the complexity of the proposed RC-JAPD becomes the lowest again, as evidenced by Fig. 4(b). This is because the SAPD's complexity increases multiplicatively as N_R increases, while only a part of RC-JAPD's complexity is affected by N_R.

IV. Performance Results

Our performance results are presented in this section. In order to investigate the EXtrinsic Information Transfer (EXIT) characteristics of the DAPSK detectors, we portray the EXIT charts [23] both of 16-DAPSK(2,8) and of 64-DAPSK(4,16) in Fig. 5. It can be seen that similar to the hard-decision-aided DAPSK's performance of Fig. 2, the JAPD and RC-JAPD exhibit an improved performance advantage over SAPD as N_R increases, which is evidenced by Fig. 5. Furthermore, Fig. 5 shows that the performance difference between the Log-MAP and Max-Log-MAP invoked by both the JAPD and SAPD is marginal. Hence the employment of the Approx-Log-MAP [24], which corrects Max-Log-MAP's approximation with the aid of a correction term stored in a lookup table is not neccessary for DAPSK detection. In this paper, we only apply the RC-JAPD and the SAPD relying on the Max-Log-MAP for the coded systems considered.

As demonstrated in Fig. 6, the soft DAPSK detectors may be invoked by our iterative demapping and decoding assisted Turbo Coded (TC) [25] systems. The half-rate TC employed is constituted by two half-rate Recursive Convolutional Codes (RSCs) associated with a constraint length of $K = 3$ (using the octal generator polynomials of [7,5]) and with the half-rate puncturing of the parity bits. In order to achieve a further improved near-capacity performance, an IRregular Convolutional Code (IRCC) of [23] amalgamated with the Unity Rate Code (URC) of [26] and our DAPSK scheme may be conceived according to the schematic seen in [27]. We summarize our simulation parameters in Table IV, where the number of iterations between the DAPSK detector and the TC/URC decoder was set to $(I_{TC-DAPSK}/I_{URC-DAPSK} = 1)$ and $(I_{TC-DAPSK}/I_{URC-DAPSK} = 2)$ for 16-DAPSK(2,8) and 64-DAPSK(4,16), respectively, because in contrast to 16-DAPSK(2,8), the 64-DAPSK(4,16) scheme has a useful iteration gain, as demonstrated by Fig. 5.

We portray the Monte-Carlo simulation based decoding trajectory in Fig. 7, which demonstrates that the IRCC-URC aided 16-DAPSK(2,8) is capable of converging at a lower SNR than the TC aided 16-DAPSK(2,8). The attainable BER performance is presented in Fig. 8, where the AMI achieved by the JAPD and the SAPD are calculated according to (17) and (19), respectively. More explicitly, the AMI seen in Fig. 8 characterizes the DAPSK detector's capability in conjunction with half-rate channel coding, which may be quantified by the E_b/N_0 value, where the DAPSK detectors' AMI achieves

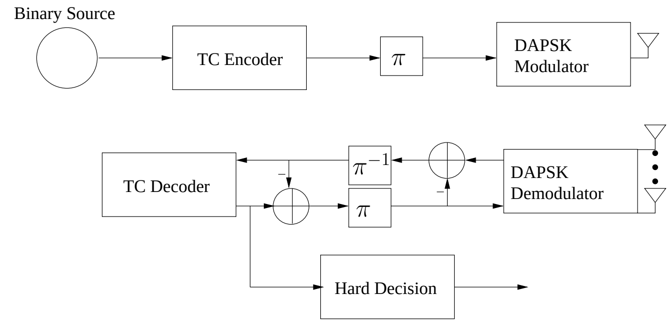

Fig. 6. Schematic of TC-aided M-DAPSK (M_A,M_P) scheme.

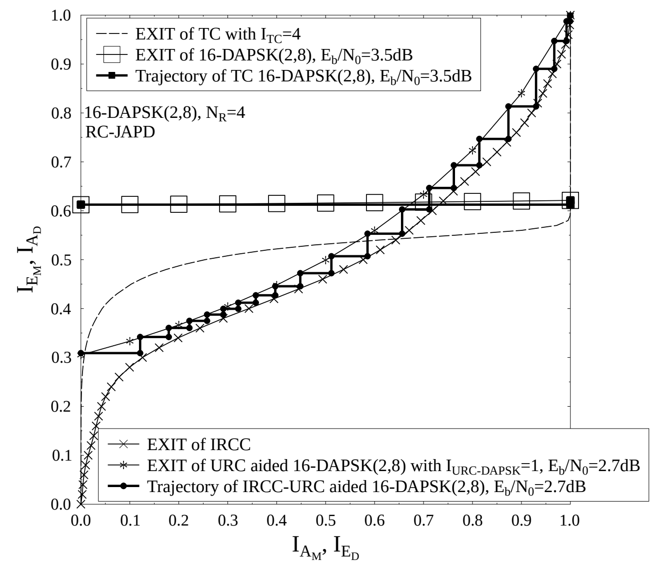

Fig. 7. EXIT charts and decoding trajectory for TC/IRCC-URC aided 16-DAPSK(2,8) detection, where the proposed RC-JAPD is invoked.

half of its maximum rate. It can be seen in Fig. 8 for both 16-DAPSK(2,8) and 64-DAPSK(4,16) that the proposed RC-JAPD outperforms the SAPD using the Max-Log-MAP by $0.9 \sim 1.4$ dB both for TC aided DAPSK scheme as well as for IRCC-URC aided DAPSK scheme, when $(N_R = 4)$ receive antennas are employed.

V. Conclusions

In this paper, we demonstrated that separately detecting the ring amplitude and phase of DAPSK imposes a performance loss, which is especially significant for soft-decision-aided DAPSK detection invoked by iterative demapping and decoding schemes relying on multiple receive antennas. As a result, compared to the SAPD of [13], the JAPD of [14] has a higher detection capability, but its detection complexity may become excessive. As a remedy, we proposed a new RC-JAPD, which links each *a priori* soft input bit to a specific part of the channel's output, so that only a reduced subset of the DAPSK constellation points has to be evaluated by the soft DAPSK detector. Our simulation results demonstrate that the proposed RC-JAPD achieves a further improved near-capacity performance (evidenced by Fig. 8), which is attained at a reduced detection complexity (evidenced by Fig. 4), when

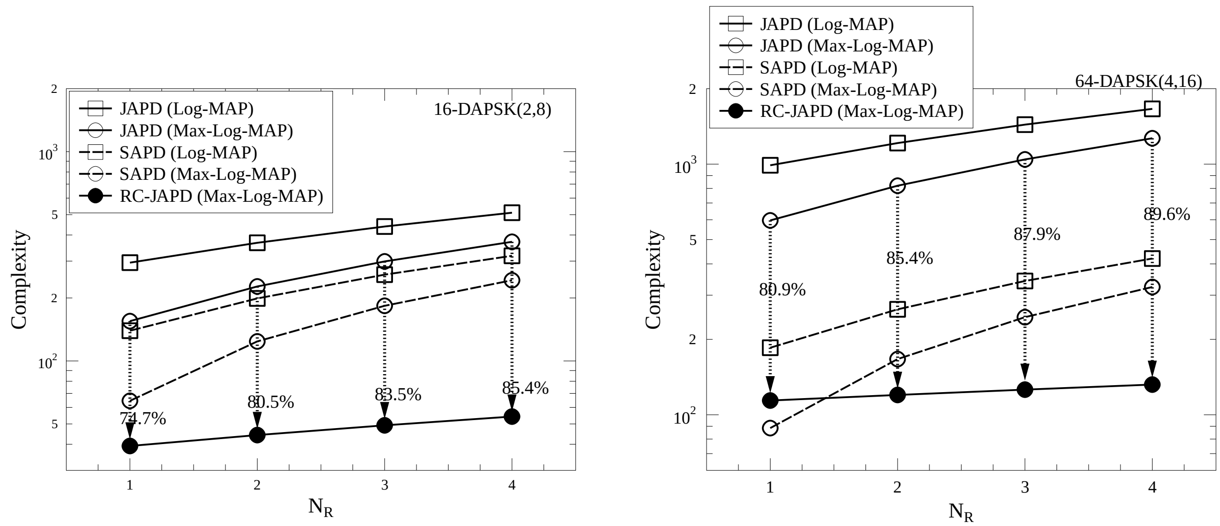

(a) 16-DAPSK(2,8)

(b) 64-DAPSK(4,16)

Fig. 4. Complexity comparison between the conventional JAPD (proposed in [14]) and SAPD (proposed in [13]) of Sec. III-A as well as the proposed RC-JAPD of Sec. III-B.

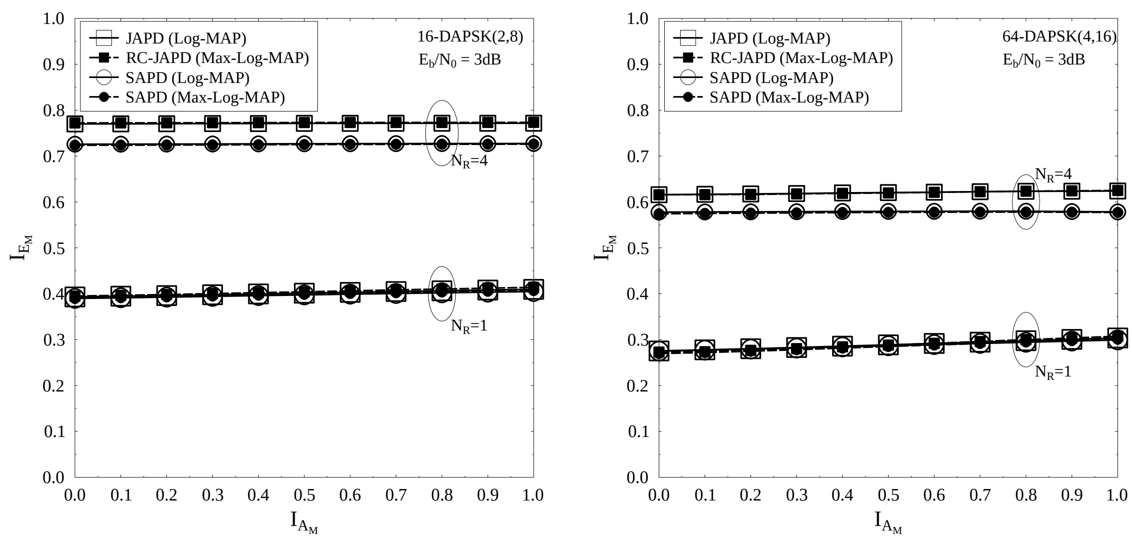

(a) 16-DAPSK(2,8)

(b) 64-DAPSK(4,16)

Fig. 5. EXIT charts of 16-DAPSK(2,8) and 64-DAPSK(4,16) invoking the JAPD, the SAPD as well as the proposed RC-JAPD.

multiple receive antennas are employed.

This contribution may be considered to be especially beneficial for cooperative communications systems [8], [19], [20], which may employ DAPSK in order to dispense with channel estimation at the relay nodes.

References

[1] S. ten Brink, J. Speidel, and R.-H. Yan, "Iterative demapping and decoding for multilevel modulation," in *IEEE Global Telecommunications Conference (GLOBECOM'98)*, vol. 1, pp. 579–584, Nov. 1998.

[2] E. Issman and W. Webb, "Carrier recovery for 16 level QAM in mobile radio," in *IEE Colloquium on Multi-Level Modulation Techniques and Point-to-Point and Mobile Radio*, pp. 9/1 –9/8, Mar. 1990.

[3] L. Hanzo, S. X. Ng, T. Keller, and W. Webb, *Quadrature Amplitude Modulation: From Basics to Adaptive Trellis-Coded, Turbo-Equalised and Space-Time Coded OFDM, CDMA and MC-CDMA Systems Digital Communications*. Wiley-IEEE Press, 2rd ed., 2004.

[4] L. Chen, H. Kusaka, and M. Kominami, "Blind phase recovery in QAM communication systems using higher order statistics," *IEEE Signal Processing Letters*, vol. 3, pp. 147 –149, May 1996.

[5] Y. Wang and E. Serpedin, "A class of blind phase recovery techniques for higher order QAM modulations: estimators and bounds," *IEEE Signal Processing Letters*, vol. 9, pp. 301 – 304, Oct. 2002.

[6] H. Rohling and V. Engels, "Differential amplitude phase shift keying (DAPSK)-a new modulation method for DTVB," in *Broadcasting Convention, 1995. IBC 95., International*, pp. 102 –108, Sept. 1995.

[7] W. Webb, L. Hanzo, and R. Steele, "Bandwidth efficient QAM schemes for Rayleigh fading channels," *IEE Proceedings I: Communications, Speech and Vision*, vol. 138, pp. 169 –175, June 1991.

Channel	Quasi-Static Rayleigh fading channels having a normalized Doppler frequency (f_d) of 0.001.
Frame length	1 000 000
Quasi-Static symbol periods	T_{QS}=11
Modulation	16-DAPSK(2,8) and 64-DAPSK(4,16).
Mapping	Gray Mapping.
Channel Coding	(1) The parallel-concatenated Turbo Code (TC) of [25] (2) The serial-concatenated IRregular Convolutional Code (IRCC) of [23] amalgamated with Unity Rate Code (URC) of [26].
TC aided DAPSK scheme	$I_{TC} = 4$ iterations within TC, $I_{TC-DAPSK} = 1$ iteration between TC decoder and 16-DAPSK(2,8) detector, $I_{TC-DAPSK} = 2$ iterations between TC decoder and 64-DAPSK(4,16) detector.
IRCC-URC aided DAPSK scheme	$I_{URC-DAPSK} = 1$ iteration between URC decoder and 16-DAPSK(2,8) detector, $I_{URC-DAPSK} = 2$ iterations between URC decoder and 64-DAPSK(4,16) detector, $I_{out} = 50$ iterations between IRCC and the amalgamated URC-DAPSK decoder.

TABLE I
SYSTEM PARAMETERS.

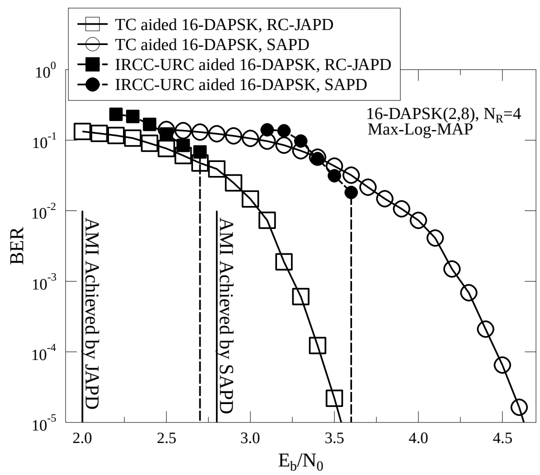

(a) TC/IRCC-URC aided 16-DAPSK(2,8)

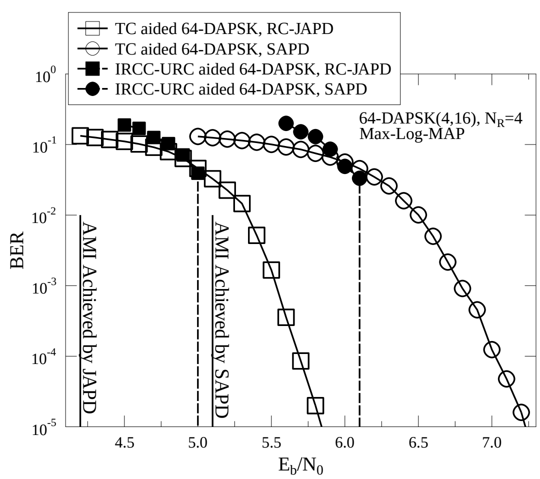

(b) TC/IRCC-URC aided 64-DAPSK(4,16)

Fig. 8. BER performance of TC/IRCC-URC aided 16-DAPSK(2,8) and 64-DAPSK(4,16) detection, where the SAPD using Max-Log-MAP and the proposed RC-JAPD are invoked.

[8] L. Wang and L. Hanzo, “Dispensing with channel estimation: Differentially modulated cooperative wireless communications,” *IEEE Communications Surveys Tutorials*, vol. PP, no. 99, pp. 1 –22, 2011.

[9] S. ten Brink, J. Speidel, and R.-H. Han, “Iterative demapping for QPSK modulation,” *Electronics Letters*, vol. 34, pp. 1459 –1460, July 1998.

[10] L. Bahl, J. Cocke, F. Jelinek, and J. Raviv, “Optimal decoding of linear codes for minimizing symbol error rate,” *IEEE Transactions on Information Theory*, vol. 20, pp. 284 – 287, Mar. 1974.

[11] J. Hagenauer and P. Hoeher, “A Viterbi algorithm with soft-decision outputs and its applications,” in *IEEE Global Telecommunications Conference (GLOBECOM’89)*, pp. 1680 –1686 vol.3, Nov. 1989.

[12] W. Koch and A. Baier, “Optimum and sub-optimum detection of coded data disturbed by time-varying intersymbol interference,” in *IEEE Global Telecommunications Conference (GLOBECOM’90)*, pp. 1679 – 1684 vol.3, Dec. 1990.

[13] K. Ishibashi, H. Ochiai, and R. Kohno, “Low-complexity bit-interleaved coded DAPSK for rayleigh-fading channels,” *IEEE Journal on Selected Areas in Communications*, vol. 23, pp. 1728 – 1738, Sept. 2005.

[14] D. Liang, S. X. Ng, and L. Hanzo, “Soft-decision Star-QAM aided BICM-ID,” *IEEE Signal Processing Letters*, vol. 18, pp. 169 –172, Mar. 2011.

[15] X. Dong, N. Beaulieu, and P. Wittke, “Error probabilities of two-dimensional M-ary signaling in fading,” *IEEE Transactions on Communications*, vol. 47, pp. 352 –355, Mar. 1999.

[16] L.-J. Lampe and R. Fischer, “Comparison and optimization of differentially encoded transmission on fading channels,” in *International Symposium on PowerLine Communication and its Applications (ISPLC’99)*, 1999.

[17] T. May, H. Rohling, and V. Engels, “Performance analysis of Viterbi decoding for 64-DAPSK and 64-QAM modulated OFDM signals,” *IEEE Transactions on Communications*, vol. 46, pp. 182 –190, Feb. 1998.

[18] D. Liang, S. X. Ng, and L. Hanzo, “Near-capacity turbo coded soft-decision aided DAPSK/Star-QAM,” in *IEEE Vehicular Technology Conference (VTC Fall)*, pp. 1 –5, Sept. 2011.

[19] J. Laneman and G. Wornell, “Distributed space-time-coded protocols for exploiting cooperative diversity in wireless networks,” *IEEE Transactions on Information Theory*, vol. 49, pp. 2415–2425, Oct. 2003.

[20] J. Laneman, D. Tse, and G. Wornell, “Cooperative diversity in wireless networks: Efficient protocols and outage behavior,” *IEEE Transactions on Information Theory*, vol. 50, pp. 3062–3080, Dec. 2004.

[21] L. Hanzo and O. Alamri and N. El-Hajjar and N. Wu, *Near-Capacity Multi Functional MIMO Systems*. John Wiley & Sons, Ltd, May 2009.

[22] S. X. Ng and L. Hanzo, “On the MIMO channel capacity of multidimensional signal sets,” *IEEE Transactions on Vehicular Technology*, vol. 55, pp. 528 – 536, Mar. 2006.

[23] M. Tuchler, “Design of serially concatenated systems depending on the block length,” *IEEE Transactions on Communications*, vol. 52, pp. 209 – 218, Feb. 2004.

[24] P. Robertson, E. Villebrun, and P. Hoeher, “A comparison of optimal and sub-optimal MAP decoding algorithms operating in the log domain,” in *IEEE International Conference on Communications (ICC’95)*, vol. 2, pp. 1009 –1013 vol.2, June 1995.

[25] C. Berrou and A. Glavieux, “Near optimum error correcting coding and decoding: Turbo-codes,” *IEEE Transactions on Communications*, vol. 44, pp. 1261 –1271, Oct. 1996.

[26] H. Tullberg and P. Siegel, “Serial concatenated TCM with an inner accumulate code-Part I: maximum-likelihood analysis,” *IEEE Transactions on Communications*, vol. 53, pp. 64 – 73, Jan. 2005.

[27] C. Xu, S. X. Ng, and L. Hanzo, “Near-capacity irregular convolutional coded cooperative differential linear dispersion codes using multiple-symbol differential detection,” *IEEE Signal Processing Letters*, vol. 18, pp. 173 –176, Mar. 2011.

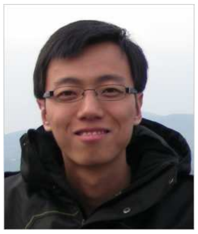

Chao Xu (S'09) received a B.Eng. degree from Beijing University of Posts and Telecommunications, China, and a BSc(Eng) with First Class Honours from Queen Mary, University of London, UK, through a Sino-UK joint degree program in 2008, both in Telecommunications Enginneering with Management. In 2009, he obtained a MSc degree with distinction in Radio Frequency Communication Systems from the University of Southampton, UK, and he was awarded IEEE Communications Society UK&RI Chapter Best MSc Student in Broadband and Mobile Communication Networks. He is currently working towards the PhD degree with the Research Group of Communications, Signal Processing and Control, School of Electronics and Computer Science, University of Southampton, UK. His research interests include reduced-complexity MIMO design, non-coherent space-time modulation detection, EXIT-chart-aided turbo detection as well as cooperative communications.

Dandan Liang received her B.Eng. degree (First class) in electronic science and technology from the PLA Information Engineering University, Zhengzhou, China, in 2008 and M.Sc. degree (First class) in radio frequency communication systems from the University of Southampton, UK, in 2009. She is currently working towards the PhD degree with the Research Group of Communications, Signal Processing and Control, School of Electronics and Computer Science, University of Southampton, UK. Her research interests include adaptive coded modulation, coded modulation, non/coherent modulation detection, iterative detection, networking coding, cooperative communications as well as wireless-optical fiber communications.

Dr Soon Xin Ng (S'99-M'03-SM'08) received the B.Eng. degree (First class) in electronics engineering and the Ph.D. degree in wireless communications from the University of Southampton, Southampton, U.K., in 1999 and 2002, respectively. From 2003 to 2006, he was a postdoctoral research fellow working on collaborative European research projects known as SCOUT, NEWCOM and PHOENIX. Since August 2006, he has been a member of academic staff in the School of Electronics and Computer Science, University of Southampton. He is involved in the OPTIMIX and CONCERTO European projects as well as the IU-ATC and UC4G projects. He is currently a senior lecturer at the University of Southampton.

His research interests include adaptive coded modulation, coded modulation, channel coding, space-time coding, joint source and channel coding, iterative detection, OFDM, MIMO, cooperative communications, distributed coding, quantum error correction codes and joint wireless-and-optical-fiber communications. He has published over 150 papers and co-authored two John Wiley/IEEE Press books in this field. He is a senior member of the IEEE, a Chartered Engineer and a fellow of the Higher Education Academy in the UK.

Lajos Hanzo FREng, FIEEE, FIET, Fellow of EURASIP, DSc received his degree in electronics in 1976 and his doctorate in 1983. In 2009 he was awarded the honorary doctorate "Doctor Honoris Causa" by the Technical University of Budapest. During his 35-year career in telecommunications he has held various research and academic posts in Hungary, Germany and the UK. Since 1986 he has been with the School of Electronics and Computer Science, University of Southampton, UK, where he holds the chair in telecommunications. He has successfully supervised 80 PhD students, co-authored 20 John Wiley/IEEE Press books on mobile radio communications totalling in excess of 10 000 pages, published 1300 research entries at IEEE Xplore, acted both as TPC and General Chair of IEEE conferences, presented keynote lectures and has been awarded a number of distinctions. Currently he is directing a 100-strong academic research team, working on a range of research projects in the field of wireless multimedia communications sponsored by industry, the Engineering and Physical Sciences Research Council (EPSRC) UK, the European IST Programme and the Mobile Virtual Centre of Excellence (VCE), UK. He is an enthusiastic supporter of industrial and academic liaison and he offers a range of industrial courses. He is also a Governor of the IEEE VTS. During 2008 - 2012 he was the Editor-in-Chief of the IEEE Press and a Chaired Professor also at Tsinghua University, Beijing. His research is funded by the European Research Council's Senior Research Fellow Grant. For further information on research in progress and associated publications please refer to http://www-mobile.ecs.soton.ac.uk.